TYPE Original Research
PUBLISHED 28 November 2025
DOI 10.3389/feart.2025.1702780



### **OPEN ACCESS**

EDITED BY
Wiwit Suryanto,
Gadjah Mada University, Indonesia

REVIEWED BY

Alessandro Vuan, National Institute of Oceanography and Applied Geophysics, Italy Bouhadad Youcef, National Earthquake Engineering Center (CGS), Algeria

\*CORRESPONDENCE Hetang Hei, ⋈ 854360354@qq.com

RECEIVED 10 September 2025 REVISED 18 October 2025 ACCEPTED 28 October 2025 PUBLISHED 28 November 2025

### CITATION

Hei H, Zhang T, Zhang Y, Wang J, Cha W, Zi C and Gao Q (2025) Characteristics and seismogenic structure of the April 2024 Weishan (Yunnan, China)  $M_{\rm S}4.1$  and  $M_{\rm S}4.3$  double-earthquake sequence. Front. Earth Sci. 13:1702780. doi: 10.3389/feart.2025.1702780

### COPYRIGHT

© 2025 Hei, Zhang, Zhang, Wang, Cha, Zi and Gao. This is an open-access article distributed under the terms of the Creative Commons Attribution License (CC BY). The use, distribution or reproduction in other forums is permitted, provided the original author(s) and the copyright owner(s) are credited and that the original publication in this journal is cited, in accordance with accepted academic practice. No use, distribution or reproduction is permitted which does not comply with these terms.

# Characteristics and seismogenic structure of the April 2024 Weishan (Yunnan, China) $M_S4.1$ and $M_S4.3$ double-earthquake sequence

Hetang Hei<sup>1,2</sup>\*, Tianyu Zhang<sup>1</sup>, Yuan Zhang<sup>1</sup>, Jun Wang<sup>1</sup>, Wenjian Cha<sup>1</sup>, Chengzhu Zi<sup>1</sup> and Qiong Gao<sup>1</sup>

<sup>1</sup>Yunnan Earthquake Agency, Kunming, China, <sup>2</sup>Northwestern Yunnan Crustal Tectonics Observatory, China Earthquake Administration. Dali. China

According to the China Earthquake Networks Center (CENC), two moderate earthquakes of M<sub>S</sub> 4.1 and M<sub>S</sub> 4.3 struck Weishan County, Yunnan Province, at 05:54:10 local time on 19 April 2024 and 13:05:16 local time on 24 April 2024, respectively, constituting a double-main-shock sequence. Using the doubledifference relocation algorithm and Cut-and-Paste (CAP) waveform inversion, we precisely located 115 events ( $M_1 \ge 0$ ) and determined focal mechanisms for the two main shocks. Integrated with regional geological mapping, our results show: (1) The sequence trends NW-SE (~8 km) with a subsidiary NE-SW lobe (~4.5 km) and hypocentres concentrated at 3-11 km depth; both shocks exhibit normal faulting with a left-lateral strike-slip component; (2) Rupture was controlled by the NE-SW-striking Bianjiang Fault and the Jijie-Longjie anticline hinge, producing a downward-converging, cone-shaped seismic cloud; (3) Static Coulomb stress change ( $\Delta$ CFF = +0.023 MPa) and magnitude parity confirm mutual triggering, consistent with a doublet rather than a foreshock-main-shock pair. Within the context of southward-migrating M > 5 earthquakes in the Lanping-Simao terrane since 2013, the 2024 Weishan doublet highlights the reactivation of inherited fault-fold intersections driven by ongoing southeastward extrusion of Tibetan Plateau crust and provides a basis for future seismic-hazard assessment

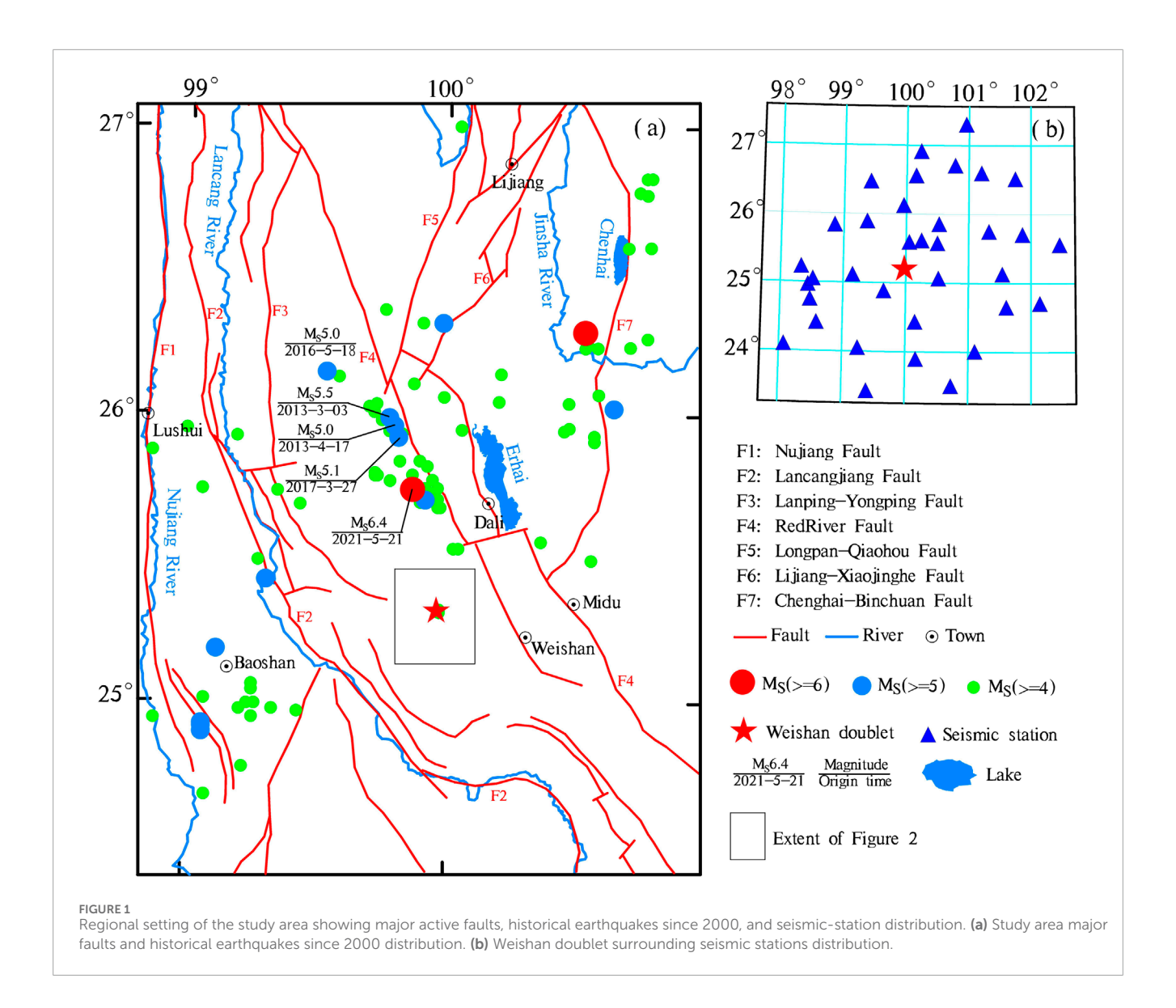
KEYWORDS

Weishan double-earthquake, earthquake relocation, focal mechanism, seismogenic structure, seismic trend

# 1 Introduction

According to the China Earthquake Networks Center, two earthquakes of  $M_{\rm S}$  4.1 and  $M_{\rm S}$  4.3 struck Weishan, Yunnan Province, at 05:54:10 local time on 19 April 2024 and 13:05:16 local time on 24 April 2024. Their epicenters lie only 2.4 km apart, defining a classic double-main-shock sequence. Field investigations report cracked masonry in the villages of Fuquma, Sijia, Xinlian, and Datangzi, as well as widespread roof-tile displacement and noticeable shaking throughout Weishan County.

The epicenters lie within the Lanping-Simao accretionary terrane on the southwestern margin of the Yangtze microcontinent. Since 2013, this terrane—particularly the belt



adjacent to the Weixi-Qiaohou Fault-has experienced a pronounced increase in moderate seismicity, including, as shown in Figure 1a, the March-April 2013 Eryuan  $M_{\rm S}$  5.5 and MS5.0 earthquakes (Zhao and Fu, 2014; Huang et al., 2015; Chang et al., 2014), the 18 May 2016 Yunlong  $M_{\odot}$  5.0 event (Jiang et al., 2019), the 27 March 2017 Yangbi  $M_S$  5.1 earthquake (Li et al., 2020), and the 21 May 2021 Yangbi  $M_S$  6.4 earthquake (Long et al., 2021; Hei et al., 2025). Notably, seismic activity is intensifying and migrating southward; yet well-documented double-earthquake sequences remain rare in this region. Motivated by these observations, we integrate high-precision earthquake relocation and focalmechanism inversion with detailed geological fieldwork to resolve the three-dimensional geometry and kinematics of the Weishan doublet. Our objectives are to (i) characterize the rupture planes of the two main shocks, (ii) quantify the interaction between these ruptures and surface-exposed faults and folds, and (iii) assess the implications for regional seismic-hazard assessment and the southward migration of large earthquakes within the Lanping-Simao terrane.

# 2 Geological setting

The study area lies within the Tethyan domain between Gondwana and Laurasia during the Paleozoic. It is situated at the junction of the Red River fault zone and the nearly N–S-trending Lijiang–Dali fault system, forming the southwestern boundary of the Sichuan–Yunnan rhombic block and a locus of concentrated stress (Li and Wang, 1975). This region is widely regarded as a principal corridor for southeastward extrusion of Tibetan Plateau material (Wu et al., 2015) and hosts a complex network of active faults.

As shown in Figure 1a, the Lanping–Simao accretionary terrane is bounded to the east by the Red River Fault and to the west by the Lancangjiang Fault. The Lancangjiang Fault is a major structure that dips steeply (50°–70°) to the southwest and displays a high-angle transpressional kinematics. Its present trace formed chiefly during the Himalayan orogeny; however, two phases of ductile shear in the Proterozoic Chongshan Group along its western margin indicate inception no later than the Indosinian. Multiphase

intermediate-acidic plutons intrude parallel to the fault and are locally offset by late-stage reactivations, attesting to long-lived structural control. Hot-spring alignment along the fault further evidences recent activity. The Weixi-Qiaohou Fault originated during the Jinning-Caledonian and cuts the crystalline basement. From Late Yanshan to Early Himalayan time it moved as a right-lateral strike-slip fault with a minor reverse component under a NE-directed maximum principal stress; during Mid-Himalayan time it retained right-lateral kinematics but deformation became dominantly brittle. Present-day geodetic and geological data indicate a transition to left-lateral motion (Liu et al., 2008). South of Midu, the fault is inferred to merge with the Red River Fault and acts as the principal conduit for crustal strain transferred from the northern Sichuan-Yunnan block (Chang et al., 2016).

Himalayan deformation within the Lanping–Simao terrane is expressed as two superposed brittle structural suites: early NW-trending folds and thrusts, and later NE-trending folds and normal faults (Liu et al., 2008). Near the epicentral area, the NE-striking Maishipo (~20 km surface trace) and Bianjiang (~20 km) faults, together with the NW-striking Chahe (~24 km) and Aju (~24 km) faults, dissect Triassic–Cretaceous mudstones and sandstones. Faults are extensively developed across the area, as illustrated in Figure 2.

# 3 Data and methods

# 3.1 Precise relocation of the earthquake sequence

Precise relocation of an earthquake sequence is the most direct way to reveal the geometry of its seismogenic structure. From the National Earthquake Catalog (http://10.5.160.18/-console/ index.action/) we extracted all events that occurred within 2 months after the main shocks (through 30 June 2024), retaining only those with  $M_{\rm L} \ge 0$  and at least six clear phase picks. Thirty-five stations within 250 km of the epicenter met this requirement; their distribution is shown in Figure 1b. All stations are equipped with three-component broadband seismometers and 24-bit digitisers sampling at 100 sps. After preprocessing, the final dataset comprised 46654 P-wave and 42839 S-wave arrival times. Earthquakes were relocated with the double-difference algorithm (Waldhauser and Schaff, 2008; Hauksson et al., 2012). This method minimizes errors arising from imperfect velocity models by inverting differential travel-time residuals between pairs of events recorded at common stations, yielding relative locations that are significantly more accurate than isolated absolute determinations (Michelini and Lomax, 2004). We adopted the 1-D velocity model derived for the Weishan-Yangbi region (Long et al., 2021) with a  $V_P/V_S$ ratio of 1.70 (Table 1). Applying this procedure to the 2-month interval following the Weishan main shocks yielded precise hypocenters for 115 earthquakes ( $M_L \ge 0$ ), including the 2  $M_S \ge 4.0$ main shocks, five events of  $3 \le M_L < 4$ , fourteen of  $2 \le M_L < 3$ , fiftyfive of  $1 \le M_L < 2$ , and thirty-nine of  $0 \le M_L < 1$ . Estimated relative uncertainties average 0.40 km in latitude, 0.34 km in longitude, and 0.70 km in depth.

Following relocation, the seismic cluster is notably compact (Figure 2). The sequence includes  $2\,M_{\rm S} \ge 4.0$  events: the 19 April  $M_{\rm S}$  4.1 shock at 25.217°N, 99.962°E, 10.61 km depth, and the 24

April  $M_{\rm S}$  4.3 shock at 25.239°N, 99.958°E, 10.49 km depth. Both epicenters align with the surface trace of the NE–SW-striking Bianjiang Fault, yet the overall aftershock distribution elongates NW–SE. To further illuminate the deep geometry of the seismogenic structure, we constructed depth-sections of the earthquake sequence along its dominant long-axis trend (profile A–A\*) and along the perpendicular direction (profile B–B\*); the surface traces of both sections are shown in Figure 2. As illustrated in Figure 3, the two profiles both reveal a systematic downward convergence of hypocentres, with larger-magnitude events preferentially located at greater depths; temporally, the sequence expands inward from both shallow and deep levels and progressively concentrates at intermediate depths.

# 3.2 Focal mechanism solutions

Focal-mechanism solutions provide the most critical seismological constraints on fault geometry and kinematics (strike, dip, and rake). A variety of inversion techniques exist-gridsearch algorithms (Reasenberg and Oppenheimer, 2017), P- and S-wave amplitude-ratio methods, first-motion polarity analysis, and the Cut-and-Paste (CAP) approach that jointly inverts bodyand surface-wave trains (Zhu and Helmberger, 1996). To resolve the seismogenic structure of the Weishan sequence we apply the CAP method to the  $2 M_S \ge 4.0$  events that yield high signalto-noise broadband waveforms. The algorithm compensates for lateral heterogeneity not captured by a 1-D velocity model by allowing independent time shifts between observed and synthetic P- and surface-wave windows (Long et al., 2010). We select threecomponent records within 300 km epicentral distance, remove the instrument response, demean and detrend the waveforms, and compute Green's functions with the frequency-wavenumber (F-K) technique (Zhu and Rivera, 2002) using the same 1-D velocity model employed for relocation. During inversion we use a 40 s P-wave window (shortened for stations within 200 km to avoid surface-wave overlap) filtered at 0.05–0.2 Hz; for events below  $M_S$ 4.0 we adopt 0.05-0.1 Hz to suppress noise. Surface-wave windows are 60 s and filtered at 0.05-0.1 Hz. A grid search is performed to determine the optimal strike, dip and rake.

Taking the  $M_{\rm S}$  4.1 and  $M_{\rm S}$  4.3 main shocks as examples, Figure 4 compares the synthetic and observed waveforms at the optimum centroid depth for all stations used in the focal-mechanism inversion; both events exhibit excellent waveform fits. The  $M_{\rm S}$  4.1 event yields a best-fit centroid depth of 7.2 km, with nodal plane I at 221°/31°/-41° (strike/dip/rake) and nodal plane II at 347.7°/70.3°/-114.4°. The  $M_{\rm S}$  4.3 event gives a centroid depth of 7.1 km, with plane I at 218°/30°/-62° and plane II at 6.5°/63.8°/-105.2°. The ~3.4 km difference between the centroid and the hypoDD hypocentral depth is acceptable because the latter represents the rupture initiation point whereas the former reflects the moment-weighted centroid of the entire rupture surface.

To verify the robustness of the solutions, we repeated the CAP inversion using the CRUST1.0 model (Laske et al., 2013) to compute Green's functions. Under this alternative velocity structure the optimum centroid depths for both events are again 7.1 km, and the corresponding nodal planes are 222°/31°/-42° and 348°/69°/-114° for  $M_{\rm S}$  4.1, and 218°/30°/-61° and 6°/64°/-104.5° for  $M_{\rm S}$  4.3. The

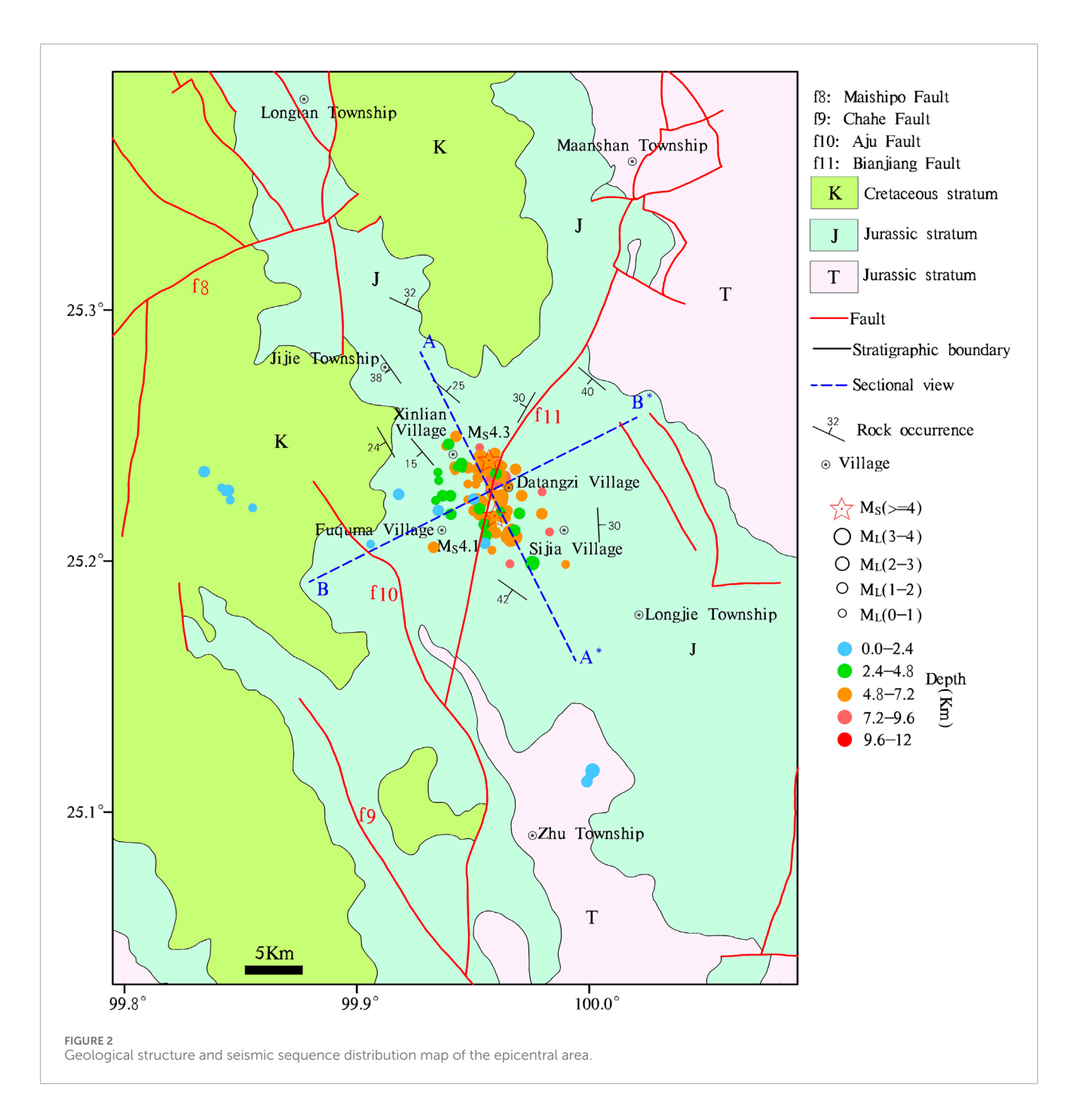


TABLE 1 One-dimensional velocity model of the Weishan-Yangbi region.

Top depth (km)	0.00	1.00	2.00	5.00	6.00	10.00	18.00	28.00	44.00
$v_p/(\mathrm{km}\cdot\mathrm{s}^{-1})$	5.36	5.45	5.88	5.93	6.02	6.05	6.26	6.46	7.82

negligible differences in depth and mechanism demonstrate that the CAP inversion is insensitive to the chosen 1-D velocity model and therefore provides stable results.

Table 2 lists the final, well-constrained focal mechanisms of the  $3\,M_{\rm S}>3.0$  events that yielded satisfactory waveform fits. Mechanisms for the remaining  $M_{\rm S}>3.0$  shocks were unstable

because of low signal-to-noise ratios in the P-wave and Rayleighwave windows and strong waveform overlap; these solutions are not reported here.

To determine whether the 19 April  $M_{\rm S}$  4.1 and 24 April  $M_{\rm S}$  4.3 events constitute a double-main-shock sequence rather than a foreshock–main-shock pair, we performed three quantitative tests.

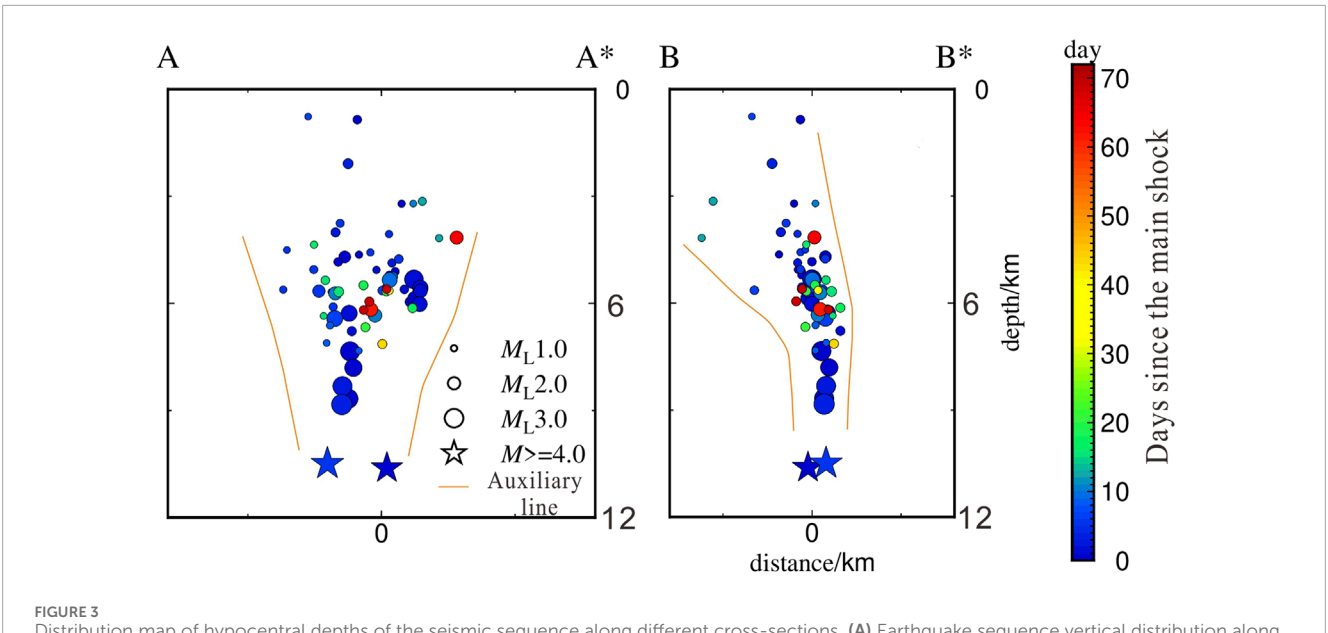
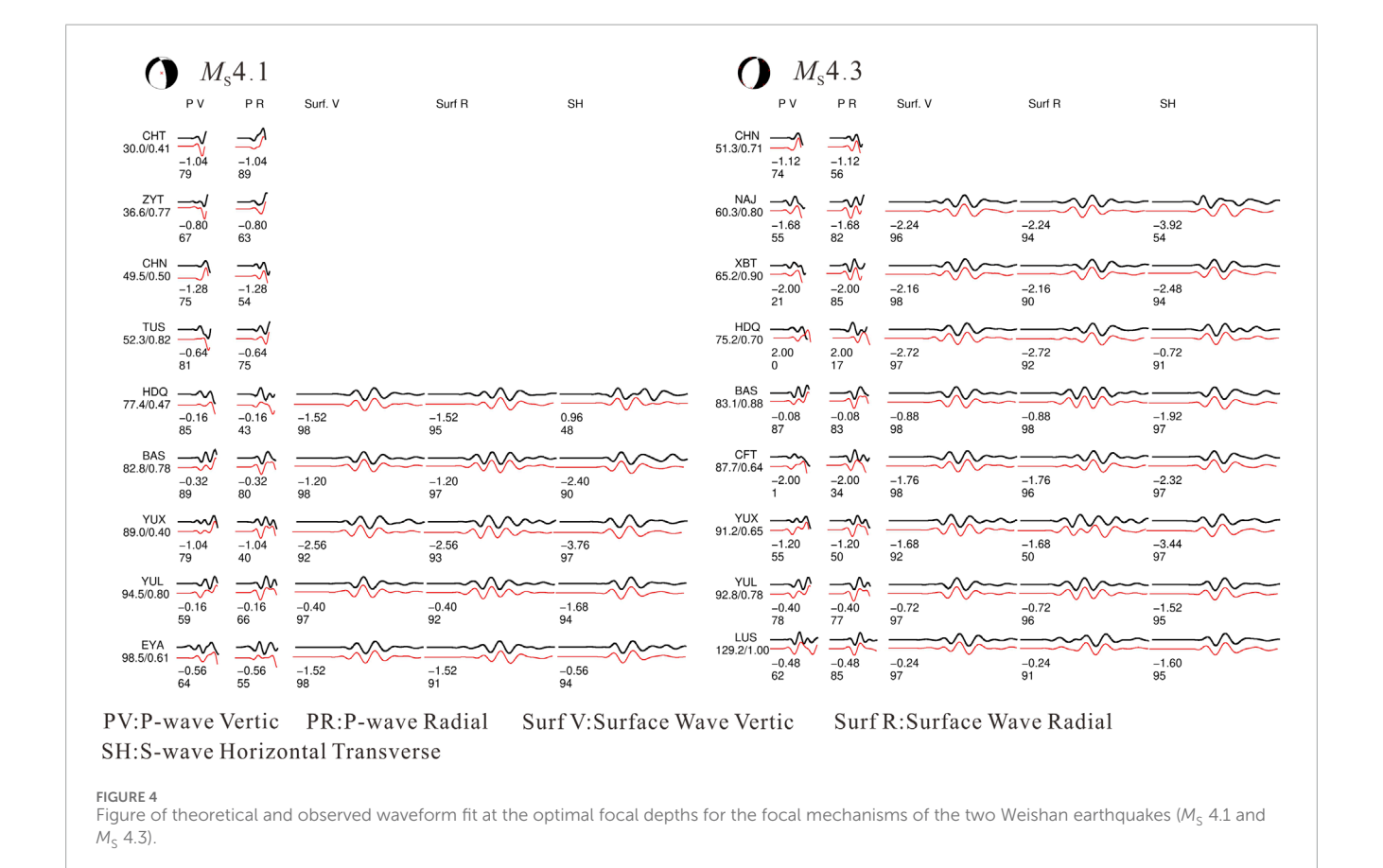


FIGURE 3
Distribution map of hypocentral depths of the seismic sequence along different cross-sections. (A) Earthquake sequence vertical distribution along A—A\*profile. (B) Earthquake sequence vertical distribution along B—B\* profile.



(i) The magnitude difference is only  $\Delta M_{\rm W} \approx 0.2$  and the second rupture released ~75% of the combined seismic moment, far above the  $\leq$ 30% typical of foreshocks. (ii) The 24 h aftershock decay of the first event follows a standard modified Omori law (p  $\approx$  1.1) without

precursory quiescence, consistent with an ordinary main shock. (iii) Static Coulomb failure stress change ( $\Delta$ CFF = +0.023 MPa) produced by the MS 4.1 rupture on the eventual  $M_{\rm S}$  4.3 nodal plane (strike 218°, dip 30°, rake –62°, depth 7.1 km) exceeds the +0.01 MPa

TABLE 2 Focal-mechanism solutions of selected M<sub>s</sub>≥3 events in the 2024 Weishan double-earthquake sequence

Nodal plane II	Rake (°)	-114.4	-104.0	-105.2	
	Dip (°)	70.3	70.0	63.8	
	Strike (°)	347.7	7.0	6.5	
Nodal plane I	Rake (°)	-41.0	-56.4	-62	
	Dip (°)	31.0	24.2	30.0	
	Strike (°)	221.0	223.1	218.0	
Depth/km		7.2	6.9	7.1	
Magnitude (M <sub>S</sub> )		4.1	3.1	4.3	
Epicenter	Latitude (°N)	25.217	25.231	25.239	
	Longitude (°E)	99.962	096'66	99.958	
Origin time (UTC)		2024-4-19 05:54:10	2024-4-19 18:47:47	2024-4-2413:05:16	

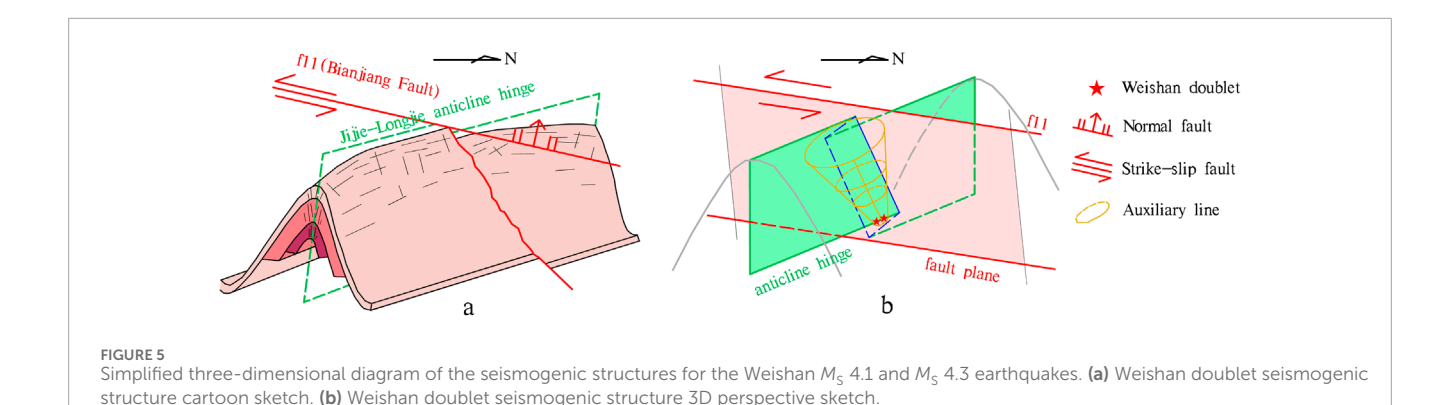
triggering threshold (King et al., 1994), and  $\sim$ 68% of the aftershock volume within 24 h experiences  $\Delta CFF > +0.01$  MPa, matching the observed seismicity burst. These combined observations satisfy the criteria for double-main-shock sequences (Kagan and Jackson, 1999), so we retain the term "doublet" throughout the paper.

# 4 Analysis and discussion

# 4.1 Seismogenic structure inference

Foreshocks and aftershocks adjacent to the main shocks commonly illuminate rupture orientation and geometry, and can therefore be employed to identify seismogenic faults following moderate-to-large earthquakes (Xu et al., 2016; Bannister et al., 2006). As shown in Figure 2, relocation indicates that both mainshock epicenters lie immediately adjacent to the surface trace of f11 (the Bianjiang Fault); however, the horizontal distribution of the sequence, although roughly symmetric across f11, trends at a high angle to the fault. To clarify this geometry, we compiled existing geological data and undertook targeted field mapping. Surface exposures of f11 exhibit variable attitudes with abundant horizontal slickensides and systematic offset of Early Triassic strata, collectively indicating a northwestward dip and a kinematic signature of normal faulting with a left-lateral strike-slip component (Liu et al., 2008). The preferred nodal planes (plane I) obtained from the focalmechanism inversions of both main shocks trend SW and are characterized by normal motion combined with left-lateral slip, in excellent agreement with f11. In addition, surface outcrops in the epicentral region consist mainly of Triassic, Jurassic, and Cretaceous strata arranged in NW-SE-trending belts (Figure 2). The earthquake sequence is largely confined to Jurassic rocks flanked by younger Cretaceous units on either side, producing a "older core, younger limbs" pattern. Measured bedding attitudes along a line connecting Jijie and Longjie townships reveal systematic dips away from this axis, defining a well-developed anticline. We therefore term this structure the Jijie-Longjie anticline (Figure 5a), which is subsequently dissected by the Bianjiang Fault. Regional correlation indicates that the Jijie-Longjie anticline is a second-order fold on the eastern limb of the larger Shishenshan synclinorium, whose NNWtrending axis (320°) is subvertical, extends >125 km, and reaches 22 km in width (Liu et al., 2008). Development of this synclinorium under horizontal compression is consistent with the contemporary regional stress field (Xu et al., 2016).

Integrating field observations, focal-mechanism solutions and precise relocations, we identify nodal plane I of both main shocks as the active rupture surface and conclude that f11 (the Bianjiang Fault) is the seismogenic fault for the Weishan doublet. In map view the earthquake sequence defines a primary NW–SE elongation ~8 km long that parallels the hinge of the Jijie–Longjie anticline; a secondary NE–SW alignment ~4.5 km long follows the Bianjiang Fault. Vertically, sections along the anticline axis (A–A\*) and the fault strike (B–B\*) (Figure 3) show hypocenters converging downward from the surface. The combined pattern forms an inverted cone whose basal ellipse has the anticline hinge as its long axis and the Bianjiang Fault trace as its short axis, centred at their intersection; as shown in Figure 5b, the 2  $M_{\rm S} \geq$  4.0 main shocks nucleate at the apex. We therefore propose that the seismogenic



structure of the Weishan double earthquake is jointly constituted by the Bianjiang Fault and the intersecting Jijie–Longjie anticline.

# 4.2 Spatiotemporal evolution of the seismic sequence

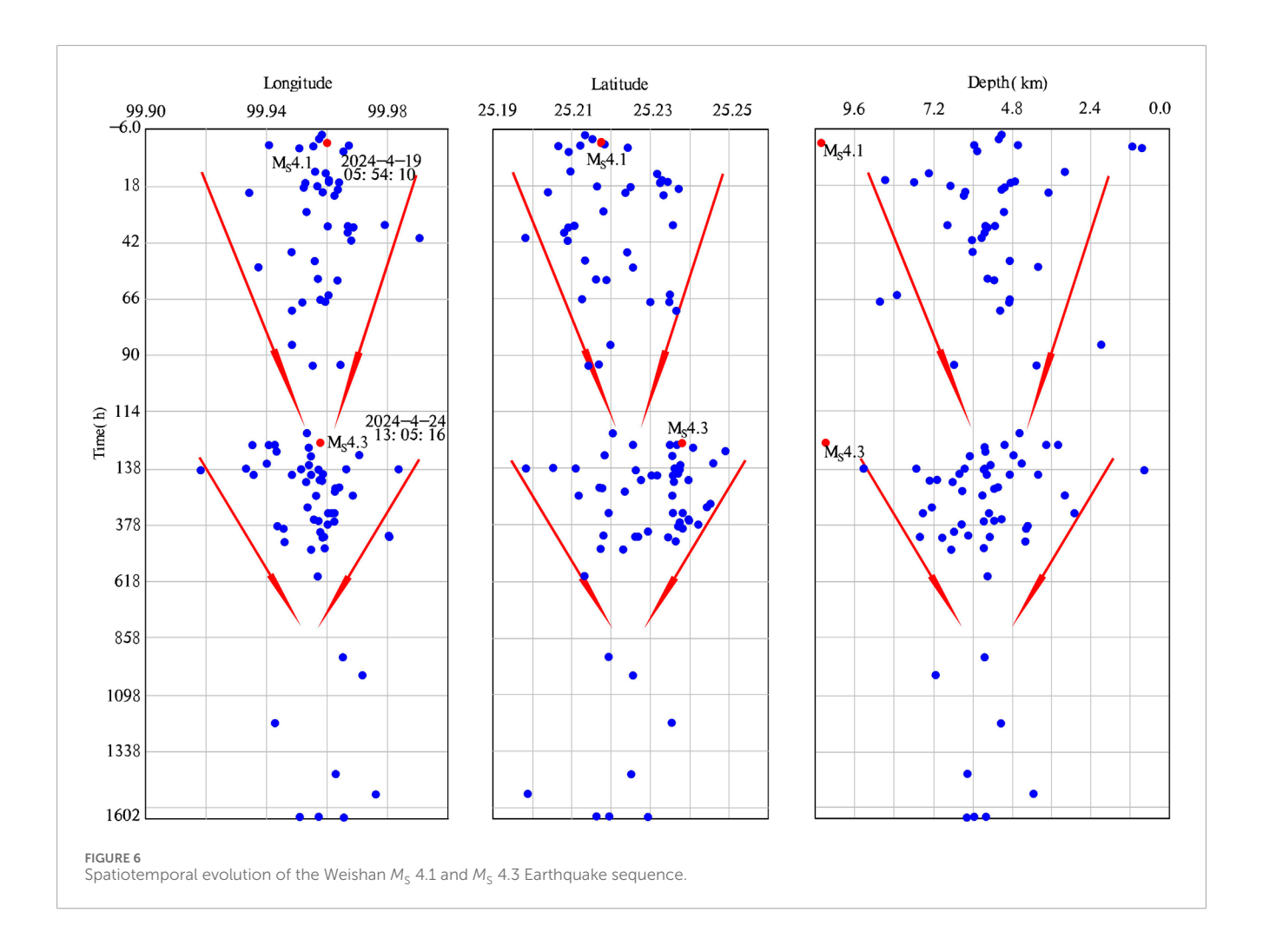
The relocated hypocenters indicate that the two Weishan main shocks are separated by ~2.4 km and by 127 h; between the main shocks and after the second main shock a number of smaller events occurred. Figure 6 plots longitude, latitude and depth of each relocated earthquake against origin time. Shortly after the first  $M_S4.1$  shock the events are dispersed in all three coordinates; with increasing time the sequence contracts toward a central locus. Following the second  $M_S4.3$  shock the same pattern repeats—outward dispersion followed by progressive convergence-until activity finally ceases. Combined with the structural interpretation, the process can be viewed as rupture spreading outward from the intersection of the Jijie-Longjie anticline hinge and the Bianjiang Fault plane, then contracting back toward that intersection. In plan view both main shocks nucleate on the fault adjacent to the convergence point, whereas in cross-section they occur at the deepest part of the entire sequence. Seismicity rates are highest during the outward-dispersed phases and decline markedly as the events collapse toward the central volume.

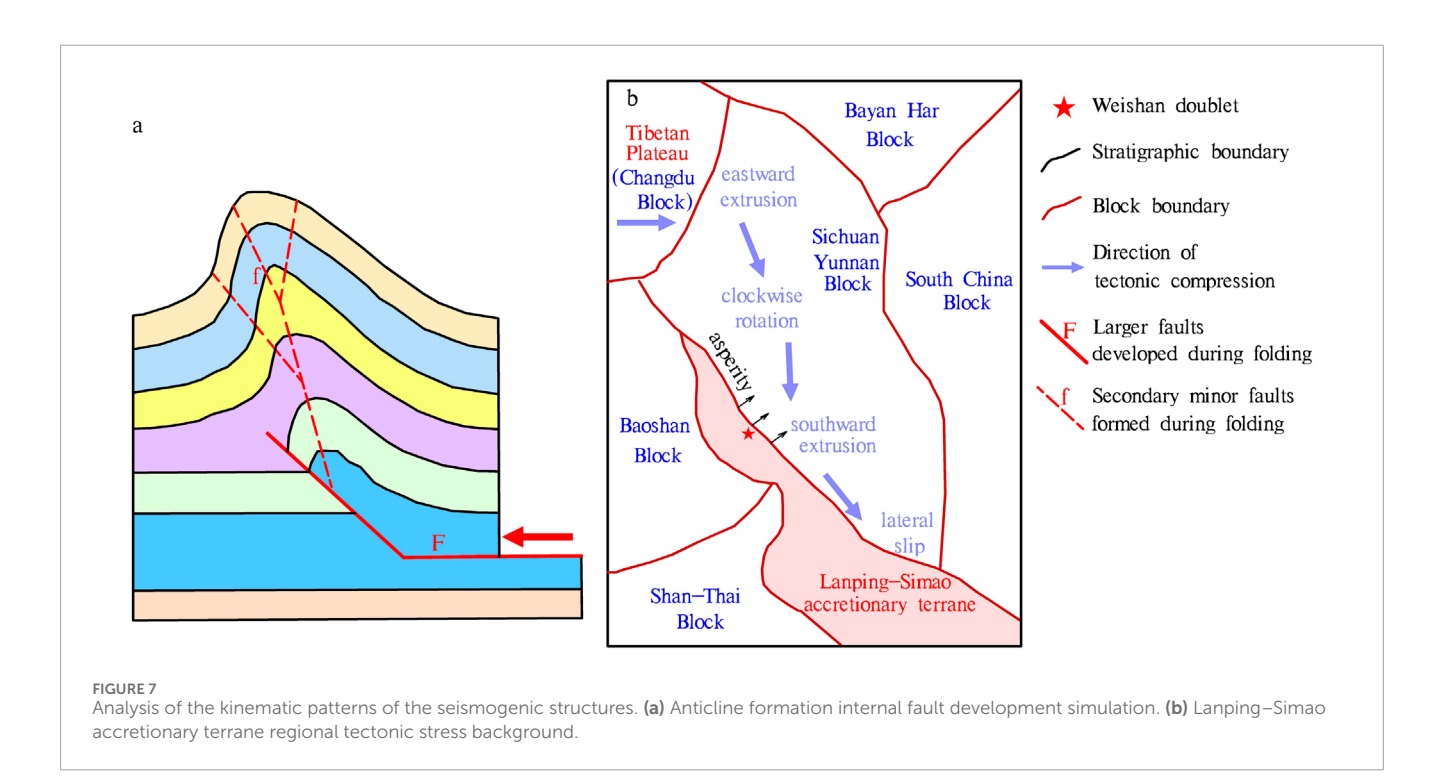
# 4.3 Possible mechanism and kinematic model of the earthquake sequence

Structural analysis shows that the distribution of the Weishan earthquake sequence is jointly controlled by the Bianjiang Fault and the Jijie–Longjie anticline. Spatiotemporal evolution exhibits two nearly identical cycles: after a strong earthquake nucleates at depth near the intersection of the anticline axis and the fault plane, aftershocks first spread outward in longitude, latitude and depth while seismicity is vigorous, then gradually converge toward the intersection as activity wanes; the sequence ends when the second main shock repeats this pattern. Each cycle represents a similar stress-release process: deep slip on the Bianjiang Fault initiates the main rupture, which then triggers conjugate fractures within the intersecting anticline and drives the subsequent aftershock expansion. Figure 7a presents a schematic

cross-section perpendicular to the preferred NW–SE elongation (profile B–B\*) illustrating the interplay between stratigraphy and faulting. According to the fault-propagation folding model with conserved bed thickness (Suppe and Medwedeff, 1990), an anticline propagates upward with fewer (as labeled "F" in Figure 7a) but larger-slip faults at depth and progressively more numerous but smaller-slip splays near the surface (as labeled "f" in Figure 7a). The depth distribution shown in Figure 3 matches this pattern perfectly: hypocenters converge downward and larger events concentrate at greater depths. Thus, under the prevailing regional stress field, the Bianjiang Fault was reactivated, simultaneously reactivating inherited faults within the Jijie–Longjie anticline. The earthquake sequence is therefore bounded by both structures, which together constitute the seismogenic framework of the Weishan doublet.

As illustrated in Figure 7b, continued southward extrusion of material along the southeastern margin of the Tibetan Plateau (Shen et al., 2005) is impeded by the Lanping-Simao accretionary terrane, subjecting the terrane to a regionally persistent north-south-directed compressional stress (Wu et al., 2015). This tectonic loading has recently triggered a series of moderate-tolarge earthquakes along the northern and western parts of the terrane and its boundaries: the March 2013 Eryuan  $M_S$ 5.5 and  $M_{\rm S}5.0$  shocks are linked to vertical displacement on the eastern master normal fault bounding the Liantie basin on the western flank of the Cangshan range (Yang et al., 2015); the 18 May 2016 Yunlong  $M_{\rm S}$ 5.0 event likely reflects activation of a newly developed NE-trending strike-slip fault within the terrane (Jiang et al., 2019); and the 21 May 2021 Yangbi  $M_S6.4$  earthquake represents renewed slip on pre-existing strike-slip faults under the current stress field (Wang et al., 2021). Similarly, in the southern part of the terrane the upper crust is accommodating the present stress regime by re-linking inherited faults, generating the 2014 Jinggu M6.6 and 2018 Mojiang M5.9 earthquakes (Wu et al., 2016; Chang et al., 2019). Reactivation of older faults within the Lanping-Simao terrane is therefore not an isolated phenomenon; instead, moderateto-large earthquake activity is progressively creating new active structures by integrating pre-existing discontinuities. In other words, obstruction of southeastward/southward Tibetan extrusion by the Lanping-Simao terrane causes repeated reactivation and reconnection of older faults, which constitutes the primary tectonic driver for the relatively frequent moderate earthquakes observed in the terrane in recent years. We therefore interpret the 2024 Weishan doublet as the result of Bianjiang Fault reactivation under the current





regional stress field, releasing accumulated strain at its intersection with the Jijie–Longjie anticline. Notably, as shown in Figure 1a, within the Lanping–Simao accretionary terrane—bounded to the west by the Lancang River fault and to the east by the Red River fault—the epicentral distances from earlier events to the 2024 Weishan doublet decrease systematically southward: the March 2013 Eryuan  $M_{\rm S}$  5.5 and  $M_{\rm S}$  5.0 pair lies ~45 km to the north, the 2016 Yunlong  $M_{\rm S}$  5.0 shock ~73 km north, the 2017 Yangbi  $M_{\rm S}$  5.1 event ~38 km north, and the 2021 Yangbi  $M_{\rm S}$  6.4 earthquake only ~13 km north. This spatial progression indicates that seismic activity within the Lanping–Simao terrane has intensified and exhibits a clear southward migration of moderate-to-large earthquakes.

Previous studies of newly formed faults and associated large earthquakes (Ding and Li, 1979; Xu, 2011) suggest that when the dynamic boundary conditions and tectonic stress field of a given evolutionary stage change, the distribution of active fault zones inherits pre-existing structures while also acquiring newly initiated features. Under such circumstances, the region contains both reactivated older faults and newly born faults that are no longer controlled by the pre-existing framework. The southeastern margin of the Tibetan Plateau, situated in a dynamically evolving stress environment, readily facilitates the reactivation and linkage of older faults, producing newborn structures that accommodate the present-day stress field. This special tectonic setting is crucial for understanding why moderate-to-large earthquakes have repeatedly occurred within the Lanping-Simao block in recent years. As Tibetan crust continues to extrude southeastward, the obstructing Lanping-Simao block generates a NNW-to-N-Soriented compressional stress field that reactivates inherited faults and nucleates new ones, a process intimately linked to the genesis of most recent earthquakes in this region. Against this geodynamic backdrop, and considering the block's lateral-slip role in buffering the Sichuan-Yunnan crustal fragment, the documented southward migration of historical earthquakes and the regional coseismic response can be used to assess future strong-motion potential. The 2024 Weishan doublet, following a series of moderate shocks within the Lanping block, demonstrates that intrablock seismicity is still ongoing and migrating southward. Given the kinematic coupling between the Lanping-Simao block, the northwestern tip of the Red River fault zone, and the Dali-Lijiang fault system of northwestern Yunnan, enhanced monitoring of moderate-to-large earthquakes in this region—especially with attention to possible future southeastward and northward migration—is imperative.

# 5 Conclusion

Employing the double-difference relocation algorithm and waveform inversion of focal mechanisms for the 19 and 24 April 2024 Weishan  $M_{\rm S}4.1$  and  $M_{\rm S}4.3$  double-earthquake sequence, and integrating detailed field geological surveys and regional data, we have characterized the spatiotemporal distribution of the sequence and elucidated its seismogenic structure and rupture processes. The key conclusions are as follows.

 The Weishan double-earthquake sequence exhibits a dominant northwest-southeast elongation ~8 km long and a secondary northeast-southwest trend ~4.5 km long, yielding an approximately elliptical horizontal distribution. Hypocentres are concentrated between 3 and 11 km depth. The relocated  $M_{\rm S}4.1$  event is positioned at 25.217°N, 99.962°E, 10.61 km depth, and the  $M_{\rm S}4.3$  event at 25.239°N, 99.958°E, 10.49 km depth. Both main shocks display essentially identical rupture characteristics, consisting of normal faulting with a left-lateral strike-slip component.

- 2. The seismogenic structure of the Weishan doublet is jointly constituted by the Bianjiang Fault and the Jijie–Longjie anticline, both of which govern the spatial pattern of the earthquake sequence. The NE–SW-striking Bianjiang Fault served as the primary seismogenic fault for the two main shocks, whereas the horizontal distribution of the sequence is aligned NW–SE by the hinge of the Jijie–Longjie anticline. Vertically, the sequence is confined by faults developed within the anticline, exhibiting downward convergence and a tendency for larger-magnitude events to nucleate at greater depths.
- 3. Viewed against the backdrop of recent seismicity within the Lanping–Simao accretionary terrane, continuous southeast-to southward extrusion of Tibetan Plateau material has forced intra-terrane structures to accommodate the evolving tectonic stress field by reactivation and linkage, thereby establishing a neotectonic framework responsible for the relatively frequent moderate-to-large earthquakes recorded in the terrane. The 2024 Weishan doublet represents the reactivation of the intersection between the pre-existing Bianjiang Fault and the Jijie–Longjie anticline under this stress regime. Consequently, future seismic-hazard assessments should prioritize detailed investigations into earthquake preparation conditions and rupture mechanisms associated with both inherited and newly formed structures within the terrane.

# Data availability statement

The original contributions presented in the study are included in the article/Supplementary Material; further inquiries can be directed to the corresponding author.

# **Author contributions**

HH: Writing – original draft, Writing – review and editing, Data curation, Project administration. TZ: Data curation, Writing – review and editing. YZ: Data curation, Writing – review and editing. JW: Methodology, Writing – review and editing. WC: Writing – review and editing. QG: Data curation, Writing – review and editing.

# **Funding**

The author(s) declare that financial support was received for the research and/or publication of this article. Earthquake Science and Technology Innovation Team of Yunnan Earthquake Agency, No. CXTD2506.

# Conflict of interest

The authors declare that the research was conducted in the absence of any commercial or financial relationships that could be construed as a potential conflict of interest.

# Generative AI statement

The author(s) declare that no Generative AI was used in the creation of this manuscript.

Any alternative text (alt text) provided alongside figures in this article has been generated by Frontiers with the support of artificial intelligence and reasonable efforts have been made to ensure accuracy, including review by the authors wherever possible. If you identify any issues, please contact us.

# References

Bannister, S., Thurber, C., and Louie, J. (2006). Detailed fault structure highlighted by finely relocated aftershocks, Arthur's pass, New Zealand. *Geophys. Res. Lett.* 33 (18), L18315. doi:10.1029/2006GL027554

Chang, Z. F., Zhang, Y. F., Zhou, Q. Y., and Chang, H. (2014). Intensity distribution characteristics and active tectonic background of the 2013 eryuan  $M_{\rm S}5.5$  earthquake. *Earthq. Res. China* 30 (4), 560–570. doi:10.3969/j.issn.1001-4683.2014.04.005

Chang, Z. F., Chang, H., Zang, Y., Mao, Z. B., and Ma, B. Q. (2016). Recent active features of weixi-qiaohou fault and its relationship with the honghe fault. *J. Geomechanics* 22 (3), 517–530. doi:10.3969/j.issn.1006-6616.2016.03.009

Chang, Z. F., Mao, Z. B., Ma, B. Q., Zhou, Q. Y., and Zhang, Y. F. (2019). The amojiang fault zone and the 2018 mojiang M 5.9 earthquake in southern Yunnan province. Geol. Bull. China 38 (6), 967–976. doi:10.3969/j.issn.1001-6616.2019.06.010

Ding, G. Y., and Li, Y. S. (1979). Seismic activity and the recent crustal fracture network of China. *Acta Geol. Sin*, 1, 22–34.

Hauksson, E., Yang, W., and Shearer, P. M. (2012). Waveform relocated earthquake catalog for southern California (1981 to June 2011). *Bull. Seismol. Soc. Am.* 102 (5), 2239–2244. doi:10.1785/0120120005

Hei, H. T., Wang, G. M., Kuang, Y. Z., Cha, W. J., and Yang, J. W. (2025). Conjugated strike-slip faults during the 21 may 2021 yangbi, Yunnan  $M_{\rm S}6.4$  earthquake sequence. China Earthq. Eng. J. 47 (1), 217–228.

Huang, X. L., Wu, Z. H., Zhao, X. Y., and Liu, F. G. (2015). Seismogenic structure of the 2014  $M_{\rm S}$  5.6 and  $M_{\rm S}$ 6.1 earthquakes in yingjiang, Yunnan province. *Acta Geosci. Sin.* 36 (1), 135–145. doi:10.3969/j.issn.1000-3025.2015.01.013

Jiang, J. Z., Li, J., and Fu, H. (2019). Seismicity analysis of the 2016  $M_{\rm S}$  5.0 yunlong earthquake, Yunnan, China and its tectonic implications. *Pure Appl. Geophys.* 176 (3), 1225–1241. doi:10.1007/s00024-018-2060-4

Kagan, Y. Y., and Jackson, D. D. (1999). Worldwide doublets of large shallow earthquakes. Bull. Seismol. Soc. Am. 89 (5), 1147–1155. doi:10.1785/BSSA0890051147

King, G. C. P., Stein, R. S., and Lin, J. (1994). Static stress changes and the triggering of earthquakes. *Bull. Seismol. Soc. Am.* 84 (3), 935–953. doi:10.1785/BSSA0840030935

Laske, G., Masters, G., Ma, Z., and Pasyanos, M. (2013). "Update on CRUST1.0 – a 1-degree global model of earth's crust,", 15. Vienna, Austria, EGU2013–EGU2658. EGU General Assem. Conf. Abstr.

Li, P., and Wang, L. M. (1975). Exploration of the seismo-geological features of the Yunnan-west sichuan region. *Chin. J. Geol.* 10 (4), 308–326.

Li, J., Jiang, J. Z., and Yang, J. Q. (2020). Microseismic detection and relocation of the 2017  $M_{\rm S}$  4.8 and  $M_{\rm S}$  5.1 yangbi earthquake sequence, Yunnan. *Acta Seismol. Sin.* 42 (5), 527–542. doi:10.11939/jass.20190130

Liu, F. G., Duan, X. D., Li, J., and Yang, Z. X. (2008). 1:250 000 dali city sheet (G47C003003) geological map and regional geological survey report. Kunming: Yunnan Geological Survey.

Long, F., Zhang, Y. J., Wen, X. Z., and Qi, Y. P. (2010). Focal mechanism solutions of  $M_{\rm L} \ge 4.0$  events in the 30 August 2008 panzhihua-huili  $M_{\rm S}6.1$  earthquake sequence. *Chin. J. Geophys.* 53 (12), 2852–2860. doi:10.3969/j.issn.0001-5733. 2010.12.007

# Publisher's note

All claims expressed in this article are solely those of the authors and do not necessarily represent those of their affiliated organizations, or those of the publisher, the editors and the reviewers. Any product that may be evaluated in this article, or claim that may be made by its manufacturer, is not guaranteed or endorsed by the publisher.

# Supplementary material

The Supplementary Material for this article can be found online at: https://www.frontiersin.org/articles/10.3389/feart.2025.1702780/full#supplementary-material

Long, F., Qi, Y. P., Yi, G. X., Zhang, Y. J., and Wen, X. Z. (2021). Relocation of the 21 may 2021  $M_{\rm S}$  6.4 Yangbi earthquake sequence and its seismogenic structure. Chin. J. Geophys. 64 (8), 2631–2646. doi:10.6038/cjg202100501

Michelini, A., and Lomax, A. (2004). The effect of velocity structure errors on double-difference earthquake location. *Geophys. Res. Lett.* 31 (9), L15614. doi:10.1029/2004GL020731

Reasenberg, P., and Oppenheimer, D. (2017). Fpfit, fpplot and fppage—Fortran computer programs for calculating and displaying earthquake fault-plane solutions (U.S. Geological survey open-file report 2017-85739). Reston, VA: U.S. Geological Survey. doi:10.3133/ofr85739

Shen, Z. K., Lü, J. N., Wang, M., and Burgmann, R. (2005). Contemporary crustal deformation around the southeast borderland of the Tibetan Plateau. *J. Geophys. Res. Solid Earth* 110 (B11), B11409. doi:10.1029/2004JB003421

Suppe, J., and Medwedeff, D. A. (1990). Geometry and kinematics of fault-propagation folding. *Eclogae Geol. Helvetiae* 83 (3), 409–454. doi:10.5169/seals-16734

Waldhauser, F., and Schaff, D. P. (2008). Large-scale relocation of two decades of northern California seismicity using cross-correlation and double-difference methods. *J. Geophys. Res. Solid Earth* 113 (B8), B08311. doi:10.1029/2007JB005479

Wang, G. M., Wu, Z. H., Peng, G. L., and Hei, H. T. (2021). Seismogenic fault and rupture characteristics of the 21 may 2021 Yangbi  $M_{\rm S}$ 6.4 earthquake: insights from sequence relocation. *J. Geomechanics* 27 (4), 662–678. doi:10.3969/j.issn.1006-6616.2021.04.011

Wu, Z. H., Long, C. X., Fan, T. Y., and Liu, F. G. (2015). The arc rotational-shear active tectonic system on the southeastern margin of the Tibetan Plateau and its dynamic characteristics. *Geol. Bull. China* 34 (1), 1–31. doi:10.3969/j.issn.1001-6616.2015.01.001

Wu, K. G., Wu, Z. H., Xu, F. K., and Chang, Z. F. (2016). Geological origin of the 2014 Jinggu earthquake swarm in southwest Yunnan: response to propagation of the Chafang-Puwen fault zone. *Geol. Bull. China* 35 (1), 140–151. doi:10.3969/j.issn.1001-6616.2016.01.012

Xu, J. (2011). Study on the newly-generated seismo-tectonic zone—A new development of seismogeological research. South China J. Seismol, 31 (4), 23–28.

Xu, Z., Huang, Z., Wang, L., and Chen, Y. (2016). Crustal stress field in Yunnan: implication for crust-mantle coupling. *Earthq. Sci.* 29 (2), 47–57. doi:10.1007/s11589-016-0145-3

Yang, J., Su, Y. J., Li, X. B., and Zhang, Y. (2015). Research on focal mechanism solutions of  $M_{\rm L} \ge 3.4$  earthquakes of the 2013 eryuan  $M_{\rm S}$  5.5 earthquake sequence. *J. Seismol. Res.* 38 (2), 196–202. doi:10.3969/j.issn.1000-0666.2015.02.005

Zhao, X. Y., and Fu, H. (2014). Seismogenic structure identification of the 2013 eryuan  $M_{\rm S}$  5.5 and  $M_{\rm S}$  5.0 earthquake sequence. *Acta Seismol. Sin.* 36 (4), 640–650. doi:10.11939/jass.2014.04.009

Zhu, L. P., and Helmberger, D. V. (1996). Advancement in source estimation techniques using broadband regional seismograms. *Bull. Seismol. Soc. Am.* 86 (5), 1634–1641. doi:10.1785/bssa0860051634

Zhu, L. P., and Rivera, L. A. (2002). A note on the dynamic and static displacements from a point source in multilayered media. *Geophys. J. Int.* 148 (3), 619–627. doi:10.1046/j.1365-246X.2002.01585.x